$Y_2O_3:Eu^{3+}, Tb^{3+}$ spherical particles based anti-reflection and wavelength conversion bifunctional films: Synthesis and application to solar cells

Ruonan Ji*, Xiaoyun Hu*, Miao Tian*, Han Linzi*, Fan Jun**, Wang Liming*, Zhan Suchang*, Zhang Qian** and Wang Yue*

* Department of Physics, Northwest University, No. 229 Taibai North Road, Xi'an, Shannxi, 710069, P. R. China, hxy3275@nwu.edu.cn

** School of Chemical Engineering, Northwest University, No. 229 Taibai North Road, Xi'an, Shannxi, 710069, P. R. China.fanjun@ nwu.edu.cn

ABSTRACT

In this study, Eu^{3+} and Tb^{3+} co-doped spherical Y_2O_3 particles were prepared via the simple, cost-effective urea homogeneous precipitation method without additives. Then, the chosen particles were added in the SiO_2 sols to get anti-reflection and wavelength conversion bifunctional films. And this bifunctional films can effectively improve the photoelectric conversion efficiency by reducing the sunlight loss and modifying the solar spectrum at the same time. Careful investigations were carried out to find the optimum preparation conditions and proper morphology. SEM photos showed that the particle sizes reduced as metal ion/urea ratio decrease. Additionally, the extracted particles turned from sphere to lamellar type when the deionized water,which was used as solvent, reduced to a certain extent. The mechanisms of the morphology formation and diversification were proposed as well. The florescent spectra indicated that the two kinds of samples shared similar florescent properties. The materials can convert a wide waveband in the UV region to visible photons from 450nm to 640nm, which just matched with high spectral response waveband of amorphous silicon solar cells, especially. And the spherical samples showed better luminous performance than the ones with lamellar morphology. In addition, the optical transmittance spectra indicated that the films adding spherial particles had better anti-reflective performances, and the best adding amount was 0.08g. Finally, the films were applied to solar cells, the photoelectric conversion efficiency enhancement can reach 10.3%.

Keywords: urea homogeneous precipitation, luminous properties, anti-reflection and wavelength conversion bifunctional films, $Y_2O_3:Eu^{3+}$, Tb^{3+} spherical particles, solar cells

1 INTRODUCTION

Solar energy, as a clean, renewable, sustainable energy, has immense potential to take place of the traditional energy source[1-2]. While the low photoelectric conversion efficiency of solar cells limit the application to a great extent. At present, anti-reflective and wavelength conversion are two predominant solutions to solve the problem [3-8]. However, technology of anti-reflective so mature that it has little promotion space, while the wavelength conversion layer exists the problem of low transmission[8]. So, combining the two method with each other to achieving complementary advantages is an effective approach to improve the the photoelectric conversion efficiency of solar cells. In this study, Eu^{3+} and Tb^{3+} co-doped Y_2O_3 spherical particles were prepared via the simple, cost-effective urea homogeneous precipitation method, without any extra additives. Then, the chosen particles were added in the self-made SiO_2 sols to get anti-reflection and wavelength conversion bifunctional film. Careful investigations were carried out to find the optimum preparation process. In addition, The mechanisms, such as the morphology formation and diversification, lumininence properity and anti-reflective performance were proposed as well.

2 EXPERIMENTAL

2.1 Preparation

In a typical experiment, appropriate amounts of Yttrium nitrate, erbium nitrate, terbium nitrate and urea were mixed with certain amount of deionized water. The mixture was ultrasonic disperse for 15min and vigorously stirred for 30 min to form a clear solution. Then, the solution was sealed and heated to 90℃ up to 2h. The resulting colloidal solutions were centrifuged at 4000 rpm for 30 min; the precipitates were washed 3 times with ethanol and deionized water and dried at 70℃ for 24 h under vacuum. Dried precipitates were then annealed in air at different temperatures for 2 h to produce oxide particles.Then, Different masses of the chosen $Y_2O_3:Eu^{3+},Tb^{3+}$ particles were dispersed in 40 mL self-made SiO_2 sols and stirred for 15 min. After ultrasonic dispersion for 30 min, the sols were dip-coated on the K9 glass substrate and dried at room temperature to get the antireflection-wavelength conversion bifunctional films.

2.2 Characterization

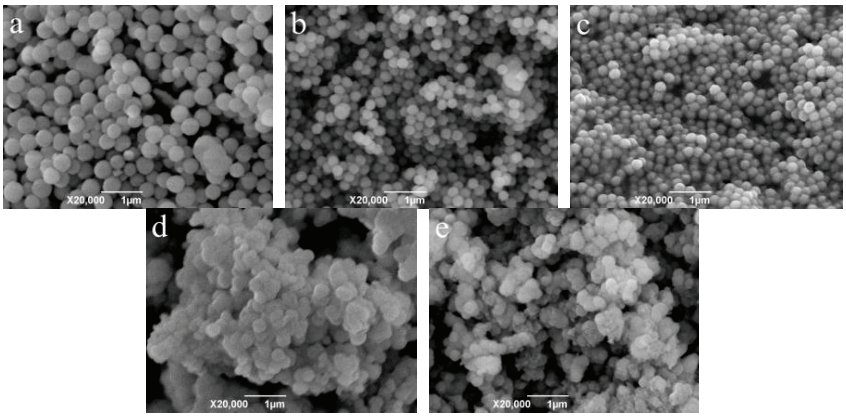

Figure1. SEM photos of samples with different metal ions/urea ratios(r) and deionized water amount(a) annealed at 1400℃ (a)r=1/5,a=200ml; (b) r=1/10,a=200ml; (c)r=1/30,a=200ml; (d) r=1/8,a=50ml; (e) r=1/20,a=50ml.

Scanning electron microscopy (SEM) images were recorded by a JEOL JSM-6390A system. The PL measurements were performed with a Hitachi F-7000 spectrophotometer equipped with a 150W Xenon lamp as an excitation source. The UV–Vis-NIR transmittance measurements of the as-prepared films were performed on a UV-3600(SHIMADZU, Japan).The photovoltaic parameters of the films were obtained by a SAC-Ⅲ Solar photovoltaic cell test system with a standard monocrystalline silicon solar cell under irradiation of a solar stimulation source (ZKY-SAC-Ⅱ Xenon lamp, 6614.85mW/m^2). All the measurements were performed at room temperature.

3 RESULTS AND DISCUSSIONS

Particles produced with different deionized water amount(a) and metal ions/urea ratios(r) are shown in Fig.1. With the amout of deionized water of 200mL, the as-prepared particles were sphere. When the metal ions/urea ratios chose 1/5(Fig1 a), the mean size of the particles was 416nm. While when lessened to 1/10(Fig1 b) and 1/30(Fig1 c), the size reduced substantially to 257nm and 245nm, respectively. Also, a densification behavior of the particles can be observed visibly. However, when the the amout of deionized water was lessened to 50mL, the morphology of the particles turned from spherical to lamellar. Whereas the particle size of the lamellar ones still following the above-mentioned rules.

The main reactions of urea homogeneous precipitation method for Y_2O_3 preparation were listed as follows.

Urea Hydrolysis

$$CO(NH_2)_2+3H_2O\rightarrow 2NH_3\bullet H_2O+CO_2\uparrow$$

Ammonia Ionization

$$NH_3\bullet H_2O\rightarrow NH_4^+ + OH^-$$

Precipitation Reaction

$$Y^{3+}+3OH^-+CO_2\rightarrow Y(OH)CO_3\bullet H_2O$$

Calcination

$$Y(OH)CO_3\bullet H_2O\rightarrow Y(OH)CO_3+H_2O$$

$$2Y(OH)CO_3\rightarrow Y_2O(CO_3)_2+H_2O$$

$$Y_2O(CO_3)_2\rightarrow Y_2O_3+2CO_2\uparrow$$

As significant amount reduce of the deionized water would lead to notable concentration increase of urea. Then following by a remarkable concentration increase of OH^- since water was still excessive, a raise of the pH of the solution appeared. The studies of Li [9] and Saito [10] show that the product is easy to form irregular morphology, such as lamellar and acicular, when the pH of the system raises to about 10. Which are match with the result of Fig1d and 1e. So the amount of the solvent can affect the morphology to some extent.

High metal ions/urea ratio means the lack of precipitator. When the concertration of the solutes actual participate in the precipitation reaction is quite low, even below the critical saturation of nucleation, no new crystal nuclei will appear and the original crystal nuclei grow up by molecular addition. So the products of higher metal ions/urea ratio easy to have larger partical size than the lower ones. While when the concertration of the solutes actual participate in the precipitation reaction reaches the critical saturation of nucleation with the decrease of metal ions/urea ratio, an instantaneous explosive nucleation will happen. A respectable sum of crystal nuclei exist in the solution, in the combined action of nucleation and volume growth, a densification behavior of the particles can be observed obviously.

Fig.2 shows the fluorescence spectra of the spherical Y_2O_3:Eu^{3+}, Tb^{3+} particles. And the lamellar particles share similar luminous properties with spherical ones (not shown). The excitation and emission spectra of Eu^{3+} doped Y_2O_3 and Tb^{3+} doped Y_2O_3 are also showed in Fig.2b and Fig.2c to distinguish the characteristic peaks of Eu^{3+} from Tb^{3+}. The material can convert a wide waveband in the UV region to visible photons from 450nm to 640nm. Amorphous silicon solar cells have high response in visible light with a peak at about 600nm, so the as-prepared materials are proper for the wavelength conversion application to amorphous silicon solar cells, especially. Upon excitation into the charge-transfer band CTB of O^{2-}-Eu^{3+} at 234 nm, the emission spectrum exhibits several emission lines (533nm, 551nm, 564nm, 581nm, 593nm, 611nm, 629nm, 650nm and 709nm) that can be assigned to the $^5D_1$-$^7F_1$ and $^5D_0$-^7F_j(where j = 0, 1, 2, 3 and 4) transitions within Eu^{3+} (and the results are shown in Fig.2c). [11-12]

Furthermore, a double excitation band between 250 and 320 nm that is assigned to charge transfer absorption from the 2p orbital of oxygen to the 4f orbital of Tb^{3+} or Tb^{3+}

intra-band ($4f^8$-4f5d) excitation is also observable in Fig. 2b. When excited at 273 nm overlaps the CTB regions of Eu^{3+} and Tb^{3+}, except the typical emission peaks of Eu^{3+}, blue and green transitions (484nm, 491nm, 541nm and 550nm) due to the characteristic $^5D_4$-$^7F_6$ and $^5D_4$-$^7F_5$ transitions within the Tb^{3+} can be observed as well. The feeble red transitions (582nm, 595nm and 623nm) originated from $^5D_4$-$^7F_4$ and $^5D_4$-$^7F_3$ of Tb^{3+} were overlapped with $^5D_0$-^7F_j (where j = 0, 1, 2) transitions of Eu^{3+}, as shown in Fig. 2c. In addition, it can be seen that all the excitation spectra (Fig.2b) consist of bands with maximums respectively located at 208nm (λ_{em}=541nm, Y_2O_3:Tb^{3+} and Y_2O_3: Eu^{3+}-Tb^{3+}) and 213nm (λ_{em}=611nm, Y_2O_3:Eu^{3+} and Y_2O_3: Eu^{3+}-Tb^{3+}), which can be attributed to the Y_2O_3 host excitation band. The general f-f transition lines of Eu^{3+} in the longer wavelength region(363nm($^7F_0$-$^5L_8$), 381nm($^7F_0$-$^5G_2$), 394nm($^7F_0$-$^5L_6$) and 415nm($^7F_0$-$^5D_3$)) are obscure due to their relatively weak intensity compared with the strong Eu^{3+}-O^{2-} and Tb^{3+}-O^{2-} CTB. The presence of the Y_2O_3 host band in the excitation spectrum indicates that there exists efficient energy transfer from Y_2O_3 host to the doped rare earth ions[13].

Fig.3 shows the luminous performance of the two kinds of morphology particals. With better monodispersion, narrower size distribution, and bigger specific surface area, the spherial particles show better luminous performance than the ones with lamellar morphology.

The excitation and emission spectra of Eu^{3+} and Tb^{3+} codoped Y_2O_3 annealed at different temperature were displays in Fig.4a. The emission intensity increased with the increase of annealing temperature. With the increase of annealing temperature the content of impurities in the sample such as -OH, NO_3^- and CH_2^- and others decreased and the crystallinity of the sample increased. The quenching of the luminescence of Eu^{3+} by the vibrations of these impurities decreased, resulting in the increase of their lifetimes and PL emission intensity[14]. The intensity of peaks at 611nm and 541nm increased nearly 14 and 18 times respectively when the annealed temperature raised from 700 to 1400 ℃.

The particles annealed at 1400℃ were added in the SiO_2 sols to get anti-reflection and wavelength conversion bifunctional films. The optical transmittance spectra indicate that the films adding spherial particles had better anti-reflective performances (as Fig.4b shows). This is due to the fact that ultrasonic treatment can uniformly disperse the prepared particles in the SiO_2 sol. After being coated, the particles, which were uniform, monodispersed and spherical, seemed to form a better light trapping structure which can effectively enhance the transmittance[15]. Moreover, the best adding amount is 0.08g, and the mean increase of the transmission in 400-1100 nm waveband is above 2%. Adding amount of 0.1g and 0.2g yielded a reduction of transmittance, which indicated that the excess particles would reduce the transmittance leading by the strong scattering.

The photoelectric conversion efficiency test was carried on the film with 0.08g spherical Y_2O_3:Eu^{3+}, Tb^{3+} added to confirmed the enhancement effect. The results show that the photoelectric conversion efficiency can increase by 10.3%. It is confirmed that this bifunctional film can effectively improve the photoelectric conversion efficiency by reducing the sunlight loss and modifying the solar spectrum at the same time.

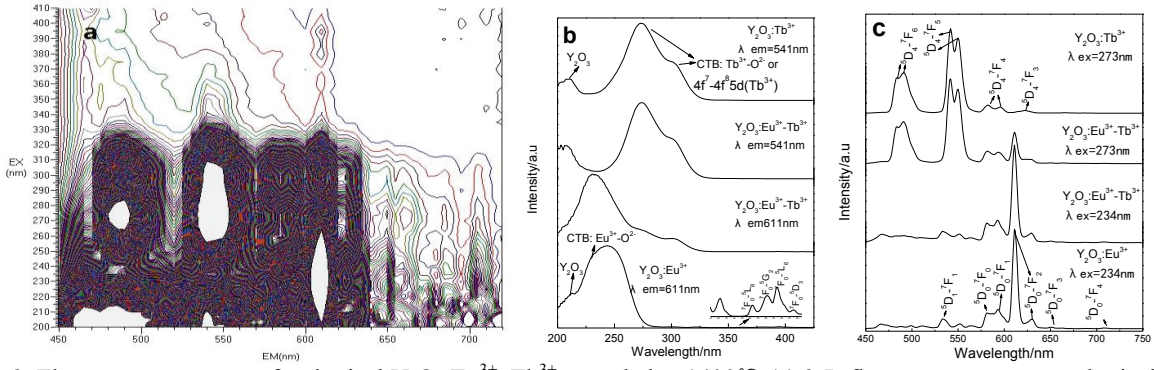

Figure 2. Fluorescence spectra of spherical Y_2O_3:Eu^{3+}, Tb^{3+} annealed at 1400℃ (a) 3-D fluorescence spectra spherical Y_2O_3:Eu^{3+}, Tb^{3+}; (b) excitation spectra ;(c) emission spectra .

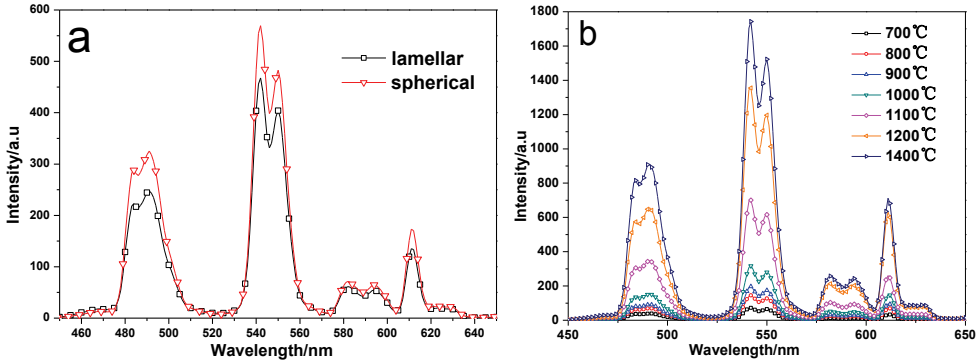

Figure 3. Emission spectrum (λ_{ex}=310nm) (a) Samples with different morphologies; (b)samples annealed at different temperatures.

CTSI-Cleantech 2013, www.ct-si.org, ISBN 978-1-4822-0594-7

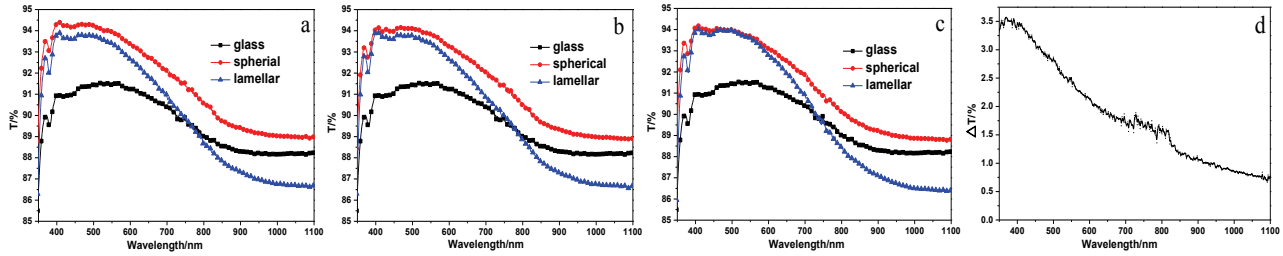

Figure 4. Optical transmittance spectra of samples adding different powders (a) 0.08g; (b) 0.1g; (c) 0.2g; (d) anti-reflection Spectrum of optimized sample.

4 CONCLUSION

In this study, Eu^{3+} and Tb^{3+} co-doped spherical Y_2O_3 particles were prepared via the simple, cost-effective urea homogeneous precipitation method without additives. The materials can convert a wide waveband in the UV region to visible photons from 450nm to 640nm, which is proper for wavelength conversion application to amorphous silicon solar cells. Then, the chosen particles were added in the SiO_2 sols to get anti-reflection and wavelength conversion bifunctional films. The mean increase of the film transmission in 400-1100 nm waveband can exceed 2% with spherical particals adding amount of 0.08g. By reducing the sunlight loss and modifying the solar spectrum at the same time, this bifunctional film can effectively improve the photoelectric conversion efficiency. The maximum enhancement can reach 10.3%.

REFERENCES

[1] Chuanwei Cheng, Hong Jin Fan, "Branched nanowires: Synthesis and energy Applications, " Nano Today, 7, 327-343, 2012.

[2] Jihuai Wu, Gentian Yue, Yaoming Xiao, Jianming Lin, Miaoliang Huang, Zhang Lan, Qunwei Tang, Yunfang Huang, Leqing Fan, Shu Yin and Tsugio Sato, "An ultraviolet responsive hybrid solar cell based on titania/poly(3-hexylthiophene), " Scientific Reports, 3,2013

[3] G. Helsch and J. Deubener, "Compatibility of antireflective coatings on glass for solar applications with photocatalytic properties," Solar Energy, 86,831–836,2012.

[4] R. Rothemund et al, "External quantum efficiency analysis of Si solar cells with II-VI nanocrystal luminescent down-shifting layers," Energy Procedia, 10, 83 – 87, 2011.

[5] G. Helsch, J. Deubener., "Compatibility of antireflective coatings on glass for solar applications with photocatalytic properties," Solar Energy, 86, 831–836, 2012.

[6] Jun-Sik Cho, Sanghun Baek, Sang Hyun Park, Joo Hyung Park, Jinsu Yoo and Kyung Hoon Yoon, " Effect of nanotextured back reflectors on light trapping in flexible silicon thin-film solar cells, " Solar Energy Materials & Solar Cells, 102, 50–57, 2012.

[7] Sark V W, Meijerink A, Schropp R., "Nanoparticles for solar spectrum conversion, " Proceed of SPIE, , 7772,1-6, 2010.

[8] Yenchi Chen, Wanyu Huang and Tengming Chen, "Enhancing the performance of photovoltaic cells by using down-converting $KCaGd(PO_4)_2$: Eu^{3+} phosphors, " Journal of Rare Earths, 29, 907-910,2011.

[9] J. G. Li, T Ikegami, J H Lee,et.al. "Co-precipaitation synthesis and sintering of yttrium alumimun garnet(YAG) powers: the effect of precipitant," J Eur Ceram Soc, 20,2395-2405,2000.

[10] N Saito, S Matsuda, T Ikegami, "Fabrication of transparent yttria ceramics at low temperature using carbonate-derived powder," J Am Ceram Soc, 81, 2023-2028,1998.

[11] Timur Sh. Atabaev, Hyung-Kook Kim, Yoon-Hwae Hwang, "Submicron Y_2O_3 particles codoped with Eu and Tb ions: Size controlled synthesis and tuning the luminescence emission, " Journal of Colloid and Interface Science, 373, 14-19,2012.

[12] Zhilong Liu, Lianxiang Yu, et.al., "Effect of Eu,Tb codoping on the luminescent properties of Y_2O_3 nanorods, " [7] Journal of Luminescence, 131,12-16, 2011.

[13] Lifan Shen, Xiao Liu, et.al., "Dynamic colour and utilizable white fluorescence from Eu/Tb ions codoped lithium-yttrium-aluminium-silicate glasses, " J. Phys. D: Appl. Phys., 45, 115301, 2012.

[14] Srirupa T. Mukherjee, V. Sudarsan, et.al., " Annealing effects on the microstructure of combustion synthesized Eu^{3+} and Tb^{3+} Doped Y_2O_3 nanoparticles, " Journal of Alloys and Compounds, 519, 9-14, 2012.

[15] P.B Chapman, M.C. Hutley, " Reduction of Lens Reflexion by the “Moth Eye” Principle, " Nature, 244, 281-282, 1973.